Modelling and simulation of the hydrodynamics and mixing profiles in the human ascending colon at different filling levels using Discrete Multiphysics

M. Schütt, K. Stamatopoulos, M.J.H. Simmons, H.K. Batchelor, A. Alexiadis

Abstract

The ascending part of the colon offers opportunities for dosage form design to prolong the release of a drug. In this work, we used computer simulations to study the hydrodynamics in this part of the colon to increase the understanding of targeted drug delivery behaviour. For this purpose, we developed and compared three different models: completely-filled colon partially-filled colon and partially-filled colon with a gaseous phase present (gas-liquid model).
The highest velocities of the liquid were found in the completely-filled model, which also shows the best mixing profile, defined by the distribution of tracking particles over time. No significant differences with regard to the mixing and velocity profiles were found between the partially-filled model and the gas-liquid model. The fastest transit time of an undissolved tablet was found in the completely-filled model. Furthermore, no significant difference between the partially-filled model and the gas-liquid model was found.

Keywords

Mathematical modelling, Peristalsis, Smoothed Particle Hydrodynamics (SPH), Fluid dynamics, Large intestine, Colon, Ascending colon, Fluid-structure interactions, Drug delivery

1. Introduction

A significant amount of research has already been carried out with respect to local drug delivery in the gastro intestinal (GI) tract [21]. However, the colon is the least researched region regarding drug absorption phenomena and local drug delivery [36], especially for the localised treatment of inflammatory bowel disease (IBD). For dosage form design, the ascending colon is the favoured part of the colon due to somewhat less variable transit times (measured with radiotelemetry capsule), and higher volumes of less viscous fluids available with respect to the transverse and descending parts of the colon [14], [23], [44].
The study of the fluid dynamics and fluid mechanics of the ascending colon, therefore, is paramount to understand the break apart, dissolution and mixing of dosage forms and the consequent design of targeted drug delivery in this part of the colon. In this regard, computational fluid dynamics has proven itself to be a valuable investigation tool (e.g. [4], [40], [41]) since it can achieve a level of detail that it is not possible by direct visualization of the actual human colon. However, with one exception [4], all computational studies performed so far (e.g. [40], [41]) refer to a completely filled colon, whereas, most of the time, the colon is only partially filled [39]. Additionally, gases are also present in the colon due to swallowed air, blood gases diffusion through the intestinal membrane, or bacterial fermentation [9], [24], [16]. The volume of gases in the ascending colon can be significant: one study [18], for instance, measured about 90% gas and 10% liquid/solid material. However, to the best of our knowledge, so far no modelling work has account for the presence of gasses in the colon.

This is a peer reviewed, accepted author manuscript of the following research article: Schütt, M., Stamatopoulos, K., Simmons, M. J. H., Batchelor, H. K., & Alexiadis, A. (2020). Modelling and simulation of the hydrodynamics and mixing profiles in the human proximal colon using Discrete Multiphysics. Computers in Biology and Medicine, 121, [103819]. https://doi.org/10.1016/j.compbiomed.2020.103819

In this paper, we used an approach similar to Alexiadis et al. [4] applied to three models describing and comparing the hydrodynamics in a completely-filled colon, a partially-filled colon and a multiphase (gas + liquid) partially-filled colon.

2. Methodology

2.1. Modelling approach

The simulations in this study are based on Discrete Multiphysics (DMP), a modelling technique also used in Alexiadis et al. [1], [2], [3] and Ariane et al. [5], [6], [7], [8]. DMP is based on coupling various particle-based modelling techniques such as Smoothed Particle Hydrodynamics (SPH), Lattice Spring Model (LSM), and the Discrete Element Method (DEM). Theoretical insights on DMP are discussed in Alexiadis et al. [1], [2]. In this study, the model accounts only for SPH and LSM. For a detailed description of the SPH method and the Lattice Spring Model (LSM), the reader can refer to [28] and [22], [29], [33] respectively.

2.2. Model geometry

In our 3D model, we investigated the ascending part of the colon of an adult human. The geometry used is a cylindrical body with a total length of 60 cm, a diameter of 5 cm and open ends. Periodic boundary conditions were used at the two ends, which means that the fluid exiting the tube on one side re-enters from the other one; this is to mimic the real-world situation of continuous transit through the colon.

Discrete Multiphysics is based on coupling various particle-based modelling techniques. In this study, SPH is used for the fluids (both liquid and gas) and LSM for the elastic membrane of the colon.

For the recording of the manometric data, we used in the model stationary SPH particles that mimic the presence of a real physical probe. In fact, in in-vivo studies, manometric data are recorded using fibre-optic catheter with sensors spaced at 1 cm [10] or water-perfused (WP) catheters with pressure sensors spaced 10 cm [27].

In Fig. 1 (a) and (b), a schematic sketch of the model, including the probe, is shown. More details are given in Table 1 and Table 2.

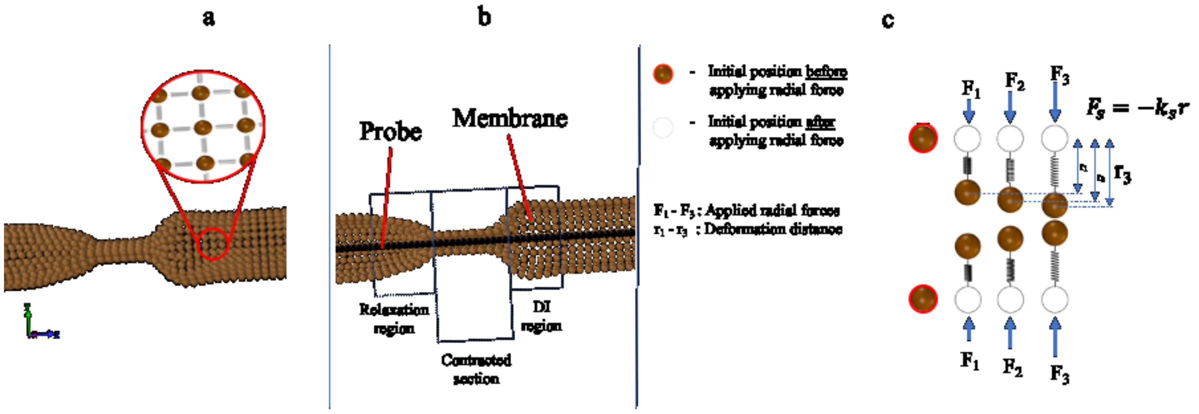

Fig. 1. (a) and (b): 3D sketch of the flexible membrane, showing the contraction and expansion of the wall. The particles representing the membrane are connected by a network of springs. The probe (catheter) for pressure measurements is

represented as black, stationary particles. (c) 2D Illustration of the elastic membrane with tethered springs at equilibrium state as well as after the application of three different radial forces (see Table 2 for details)

2.3. Model and simulation parameters

In our model, the membrane is built of 2,500 LSM particles spaced of 6.28 x 10^{-3} m and its particles are anchored to their initial position with a Hookean force (Fig. 1 (c)). The structure and hence the number of membrane particles is a compromise of complexity and performance of the model. The number of SPH particles representing the fluid varies due to the different filling levels from model to model as shown in Table 2.

The probe records the pressure along the tube every 2.5 cm. This distance was chosen to get a reasonable pressure profile for the comparison of our model with experimental data.

In our model, we used a liquid inside the colon with a viscosity similar to the viscosity (see Table 1) used in in-vitro studies in the literature [42]. Although in the real case the fluid is likely to be non-Newtonian, in this work, for simplicity, it is assumed Newtonian.

For the evaluation of the influence of a gaseous phase we used the partially-filled model and added SPH particles, representing the gas. The pressure of the gaseous phase in the colon is not well known. According to Kurbel et al. [24], the total gas pressure due to bubble formation in the colon is at atmospheric pressure or slightly above. In the model, we assume a gauge pressure of 60 Pa. Chemically, the model assumes that the gas phase is comparable to dry air and follows the equation of state for ideal gasses: technically speaking this is not true, but given the small gauge pressure, we assume that this is an acceptable simplification. Gravity acceleration in the *y*-direction is also added to all particles.
For the simulations in this study, we used three different models: completely-filled colon, partially-filled colon and gas-liquid model. The numerical values we used for the different models and simulations are listed in Table 1 and Table 2.

Table 1: Fundamental model parameters used in all simulations: for more details on the physical and mathematical meaning of the simulation parameters h, c_0, k_b and k_v, the reader is referred to [22], [28], [29], [33].

Parameter	**Value**
SPH	
Number of SPH membrane particles (1 layer)	2500
Number of SPH probe particles	134
Initial distance among particles Δr	6.28 x 10^{-3} m
Smoothing length h	9.42 x 10^{-3} m
Artificial sound of speed c_0	0.1 m s^{-1}
Time-step Δt	5 x 10^{-4} s
Density (liquid) $\rho_{L,0}$	1030 kg m^{-3}
Density (gas) $\rho_{G,0}$	1.2 kg m^{-3}
Dynamic viscosity (liquid) $\eta_{L,0}$	0.525 mPa s
Dynamic viscosity (gas) $\eta_{G,0}$	1.84 x 10^{-5} Pa s
LSM	
Hookian coefficient k_b (membrane)	0.2 J m^{-2}
Viscous damping coefficient k_v (membrane)	1 x 10^{-2} kg s^{-1}
Equilibrium distance r_0	6.28 x 10^{-3} m

Table 2: Specific model parameter for the different models

SPH Parameter	Value
Completely-Filled model (100% liquid volume)	
Number of SPH liquid particles	29728
Mass of each particle (solid)	3.9×10^{-4} kg
Mass of each particle (liquid)	3.2×10^{-5} kg
Radial contraction force F	1.280×10^{-3} N
Partially-Filled model (40% liquid volume)	
Number of SPH liquid particles	8142
Mass of each particle (solid)	3.9×10^{-4} kg
Mass of each particle (liquid)	2.42×10^{-5} kg
Radial contraction force F	0.942×10^{-3} N
Partially-Filled with a gaseous phase present (40% liquid and 60% gas volume)	
Number of SPH liquid particles	8188
Number of SPH gas particles	627
Mass of each particle (solid)	3.9×10^{-4} kg
Mass of each particle (liquid)	3.9×10^{-5} kg
Mass of each particle (gas)	4.55×10^{-7} kg
Radial contraction force F	0.9677×10^{-3} N

2.4. Colon contraction

The effect of the contraction of the colonic muscles upon the motion of the fluid inside the colon was investigated through the simulations. In humans, there are different patterns (waves) of contractions. Here, we focus on the High Amplitude Propagating Pressure Wave (HAPW) [38], [13], which transports the digested materials along the colon. The membrane of the colon consists of two muscle layers, which are the circular and the longitudinal muscle layers. The contraction of the circular muscle cells leads to a partially or completely occlusion of the lumen, and therefore an effective mixing as they propagate. The contraction of the longitudinal muscle leads to a shortening of the length of the colon and has thus minimal mixing and propulsive functions [38]. The actual shape of a peristaltic wave is still unknown and therefore modelled as an estimate according to the data available. For simplicity, and the limited influence of the longitudinal muscle, in respect to mixing and propulsion of the intestinal content [38], the contraction itself is modelled as a local contraction/activation of the circular muscle which propagates along the colon. The contraction wave (peristalsis) is modelled according to manometric measurements of HAPWs, which show a contraction time of about five seconds [17] and a propagation velocity of about one meter per second [11], [27], [38]. The HAPW is the only wave type that invariably occludes the lumen completely and additionally produces a feature called Descending Inhibition (DI), where the region in front of the bolus actively relaxes [38]. These characteristics were also implemented in the model; the contraction is modelled by applying a radial force to the membrane particles that, in our simulation, is represented by a ring of 25 particles. Each ring represents one circular muscle fibre, which can be activated independently. The numerical value of the radial force is chosen to allow full closure of the intestinal lumen avoiding interpenetration of the membrane and probe computational particles, which would result in sudden and unrealistic pressure peaks. The same HAPW is used in all three models.

2.5. Software

The open source code LAMMPS [35], [20] is used for the numerical calculations. The open source code of OVITO [43] is used for the visualisation and postprocessing of the simulation data.

3. Results and Discussion

3.1. Comparison with manometric data and other studies

To assess the model, we compared our recorded pressures with the pressure profiles from experimental manometric measurements [11]. The absolute pressure is different because our model refers to a shorter section of the colon with periodic boundary conditions.

Therefore, in Fig. 2 we compare the experimental data with the simulations based on relative pressure:

$$p^* = \frac{p}{p_0}, \tag{1}$$

where p is the experimental or simulation pressure (Pa) and p_0 the reference pressure, which is the maximum pressure in the experiment (16,430 Pa) and in the simulation (1,260 Pa).

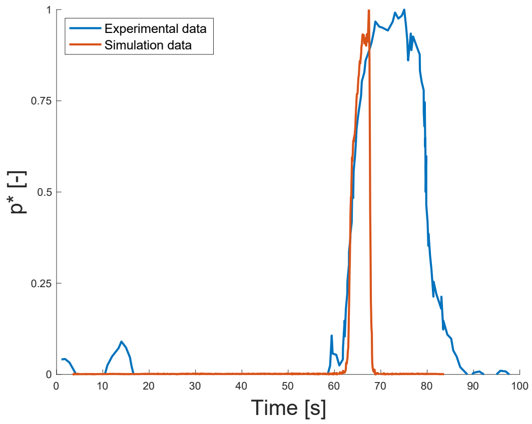

Fig. 2. Comparison between manometric measurements from [11], and simulation data from our completely-filled model.

The pressure peak in the manometric data and in the simulations is similar (Fig. 2). However, it looks like the contraction in the simulation is cut short with respect to the manometric data. In our model, the contracting section (Fig. 1 (b)) is around three/five times shorter than the real one [31], [32]. This is due to the periodic boundary conditions; in fact, if the contracting section is too large, there would be not enough room for the displaced liquid. However, this difference is only expected to affect the length of the contracting section and not the hydrodynamics in the relaxing and DI region (Fig. 3).

Fig. 3 shows an example of a peristaltic contraction travelling in antegrade direction (in our model, from left to right). The higher velocities are in the DI region, directly in front of the peristaltic wave. In this region, we can observe the formation of a vortex under peristaltic flow conditions as also reported by other studies [15], [40].

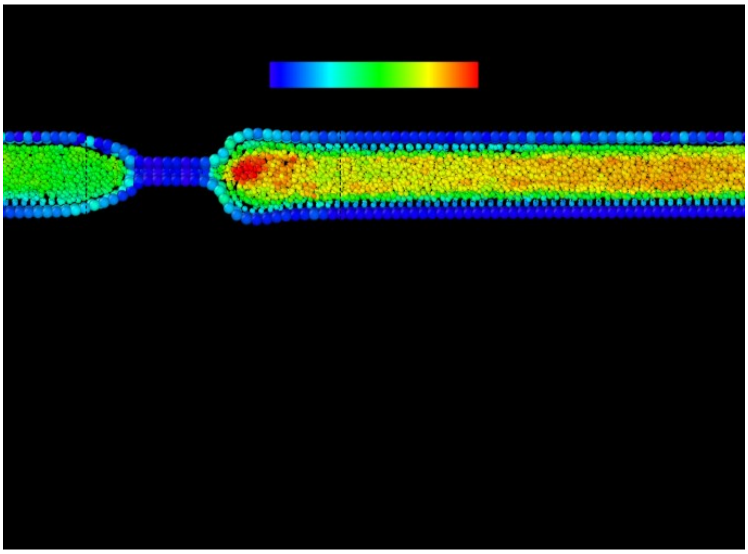

Fig. 3. Representation of a peristaltic wave. In the enlarged section, the formation of a vortex is shown in a vector representation, where the direction of the vectors indicates the flow direction respectively.

3.2. Comparison of completely-filled model with partially -filled model

The magnitude of the applied contraction force is in the partially-filled model smaller than in the completely-filled model to achieve the same pressure measurements. This is due to the fact that fully-contracting a partially-filled colon, in fact, is easier than contracting a completely full colon. The partially-filled model also shows the formation of vortices as presented in Fig. 4.

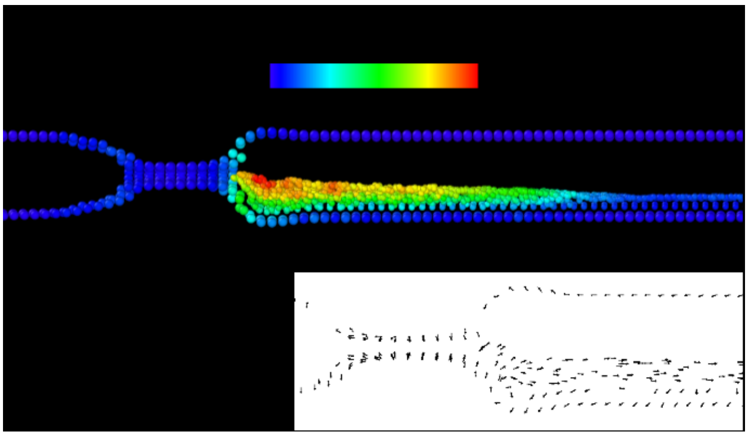

Fig. 4. Representation of a peristaltic wave in the partially-filled model. The enlarged section shows the formation of a vortex in the DI region.

Compared to the completely-filled model the velocities are smaller. As shown in Fig. 5, the velocities of the liquid particles are in both models different. They differ in magnitude as well as in the distribution over time.

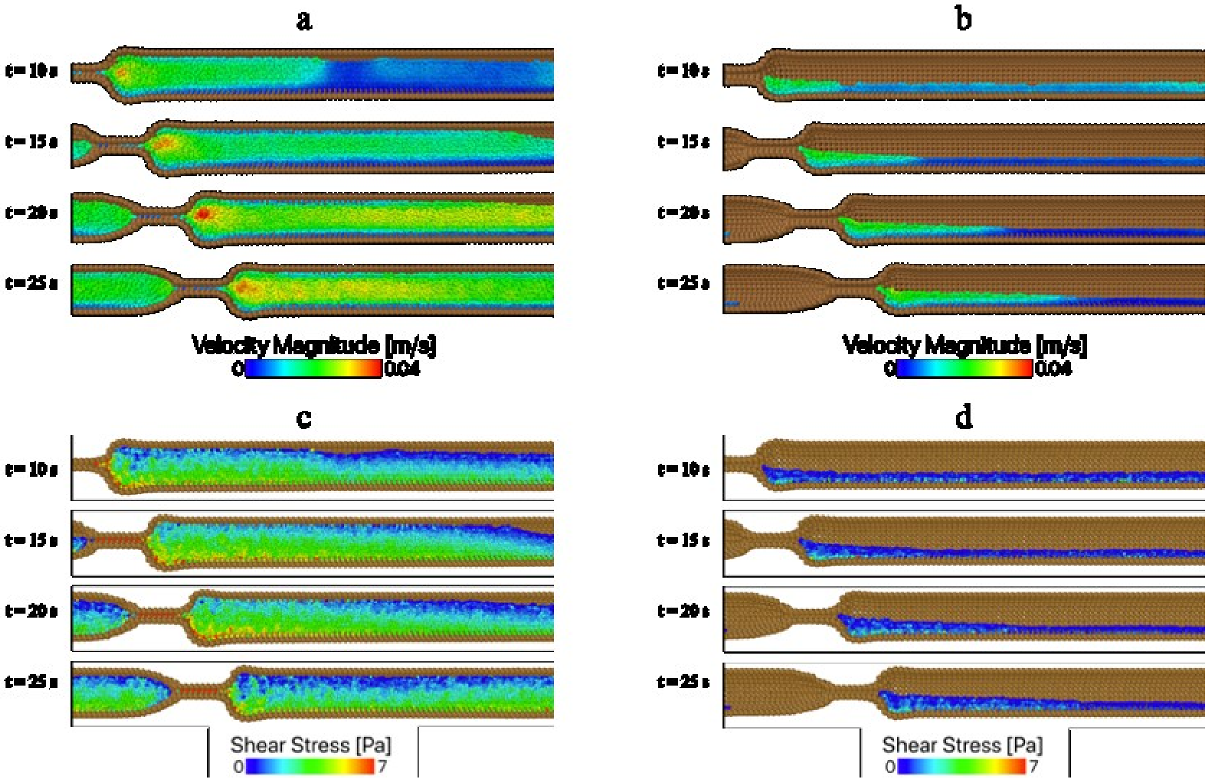

Fig. 5. Comparison of a peristaltic wave with content coloured by the velocity magnitude and shear stress, where (a) and (c) show the completely-filled model and (b) and (d) the partially-filled model.

The highest velocities in the completely-filled model arise in the centre of the tube, while in the partially-filled model the highest velocities occur on liquids free surface. Moreover, the vortex in the completely-filled model (Fig. 5 (a)) is more pronounce than in the partially-filled model (Fig. 5 (b)), which we can trace to the higher velocities found in the DI region.

Also the shear stresses in the completely-filled model (Fig. 5 (c)) are higher than in the partially-filled model (Fig. 5 (d)). In both models, the highest shear stresses are found in the lower part of the DI region where the contraction leads to an active movement of the membrane and pushes the fluid.

For the disintegration of a solid dosage form, e.g. tablets and thus the release of drug particles containing the Active Pharmaceutical Ingredient (API), the shear stress is an essential parameter [26]. A higher shear stress acting on the tablet leads to a faster breakage and a corresponding faster release of the API.

Once the API has been released the mixing profile is important for the distribution of the API and thus has a direct influence on the successful treatment.

For a visually representation of the difference in the mixing performance of both models, we track the evolution of a group of fluid particles (red particles in Fig. 6).

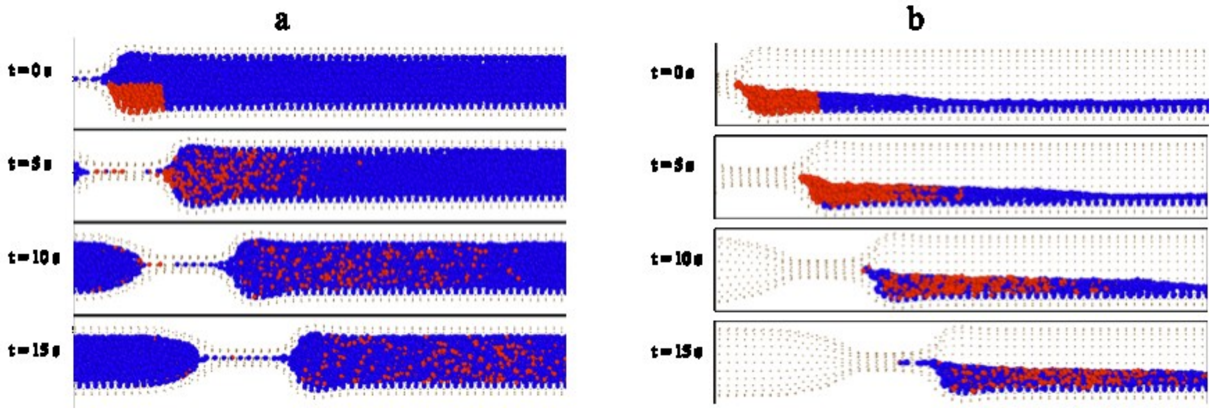

Fig. 6. Mixing profile of (a) completely-filled model and (b) partially-filled model with tracking particles (red coloured) at different time-steps.

After 5 seconds, the distance travelled by the tracking particles is almost identical in both models.
After 10 seconds, the tracking particles in the completely-filled model cover a distance of about 20% more than in the partially-filled model and the particles in the completely-filled model are more spread out.
After 15 seconds, in the completely-filled model, the particles are uniformly distributed, while the partially-filled model still shows some patches of higher concentration.

Drugs and medicines are administered in a wide variety of forms as tablets, as capsules, as granulates, as a liquid or as a foam [19], [34]. Some of these forms (e.g. emulsions and suspensions of micro- and nanoparticles in which the API is finely dispersed) are dispersed in the luminal content and, therefore, behave like the tracking particles discussed above.
Studies with a time dependent API release showed an increase in IBD treatment success [25]. A time depending release results in a low but constant API concentration along the colon which is comparable with the mixing profile of our completely-filled model. The tracking particle are distributed faster along the colon which results in an increased exposure time of API. In Fig. 6, we discussed dosage forms that are finely dispersed in the luminal content. The opposite scenario occurs when the drug is released slowly like the case of a tablet that is not very soluble in the luminal content. In Fig. 7, we consider the extreme scenario of an insoluble tabled. The tablet is cylindrical with a diameter of 10 mm, a height of 5 mm and neutrally buoyant. Fig. 7 compares the trajectory of the tablet among the completely-filled model, the partially-filled model and the gas-liquid model.

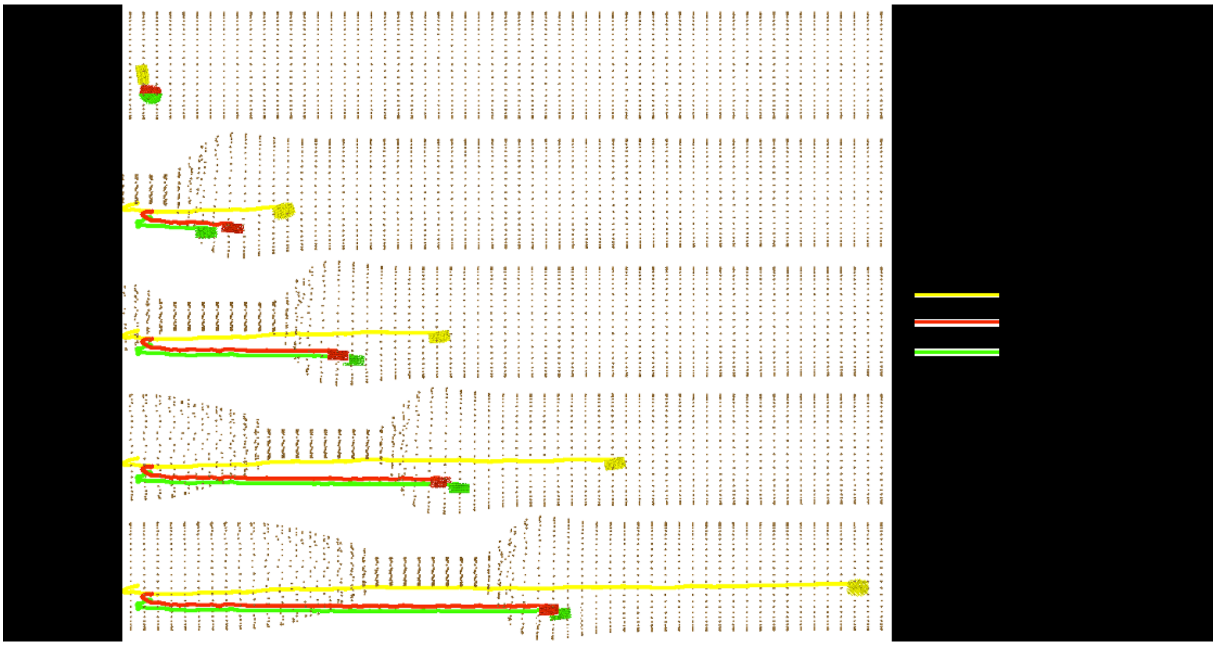

Fig. 7. Visualisation of the time dependent trajectory of a tablet in the different models.

The trajectory of the tablet is recorded from the moment the peristaltic wave begins. In all models, the tablet initially moves slightly to the left before being pushed by the peristaltic wave in the direction of propagation.

In the completely-filled model, the tablet remains its initial position, whereas in the partially-filled model and the gas-liquid model the tablet is pushed by the peristaltic wave (swirl) to the bottom of the colon. The velocity of the tablet in the partially-filled model and the gas-liquid model are approximately equal. At the beginning (10 seconds) the velocity of the tablet in the partially-filled model is slightly higher than in the gas-liquid model, but this changes between 10 seconds and 15 seconds, so that the distance travelled by the tablet in the gas-liquid model is greater than in the partially-filled model. From 15 seconds on, the velocity of the tablet in the partially-filled model and the gas-liquid model are about the same. The highest tablet velocity was found at all times in the completely-filled model.

3.3. Influence of a gaseous phase present

Fig. 8 (a) and (b) shows the particles representing the liquid and gaseous phase, respectively, coloured by the velocity magnitude, caused by a peristaltic wave at different timesteps. Fig. 8 (c) represents the shear stress occurring in the liquid phase.

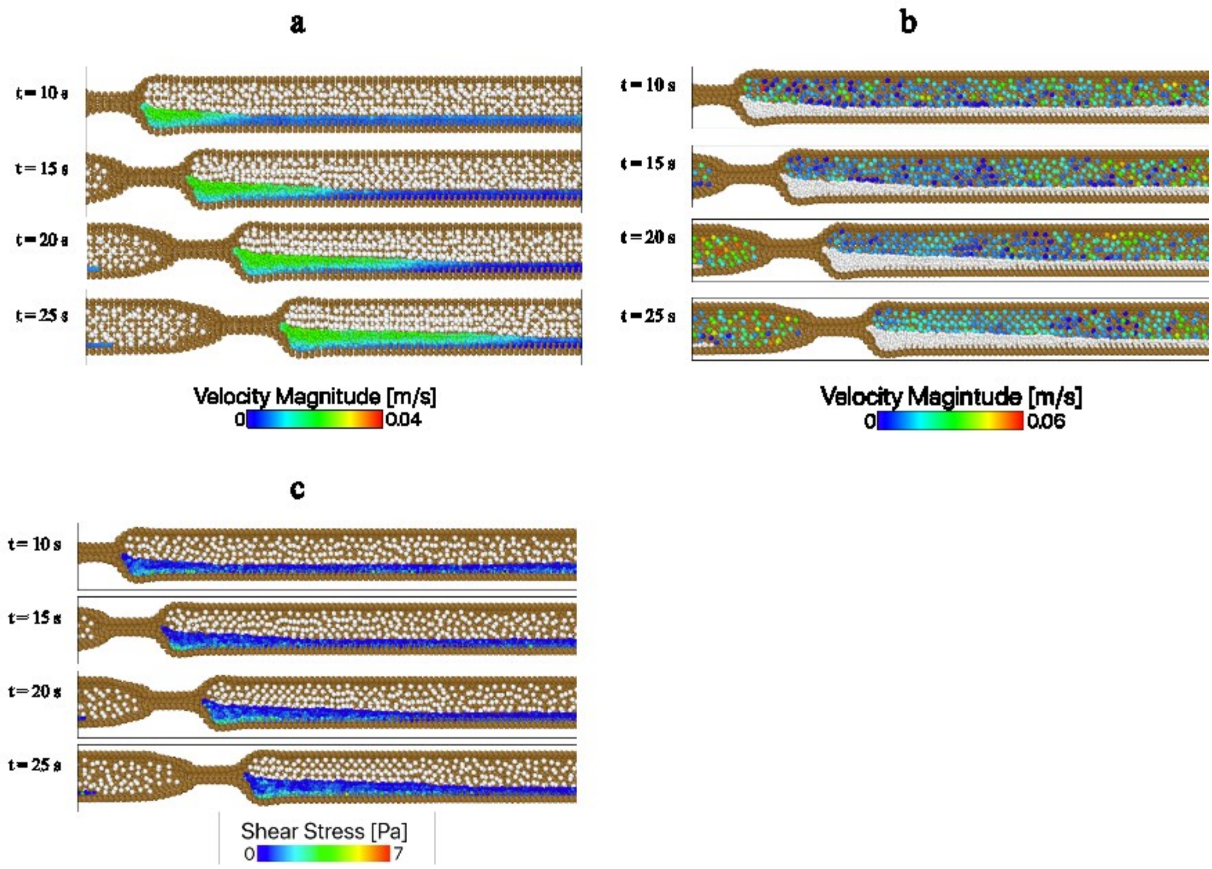

Fig. 8. (a) and (b) Comparison of a peristaltic wave with content coloured by the velocity magnitude in the gas-liquid model. In (a) the velocities of the liquid phase and in (b) the gaseous phase are analysed. (c) Representation of the shear stresses in the liquid phase.

The liquid phase (Fig. 8 (a)) shows almost the same velocities as seen in the partially-filled model (Fig. 5 (b)). After 25 seconds the velocity in the gas-liquid model is slightly higher along the colon compared to the model without a gas phase. The velocity magnitude of the gaseous phase (Fig. 8 (b)) in front of the peristaltic wave stays in the range of the propagation velocity of the peristaltic wave. Except the gas particles entering on the left side again (e.g. at 20 seconds and 25 seconds) show a slightly increased velocity magnitude.
Also the shear stress in the liquid phase (Fig. 8 (c)) shows almost the same distribution and magnitude as seen in the partially-filled model (Fig. 5 (d)). As there are no significant differences, it can be assumed that the gas phase has less or no influence in the shear stresses that occur.

From Fig. 9 (a) it can be seen that the velocity magnitude of the gaseous phase in front of the peristaltic wave is relatively constant and the arrows show a quite linear flow pattern. The gas particles entering on the left-hand side whereas showing higher velocities and swirl.

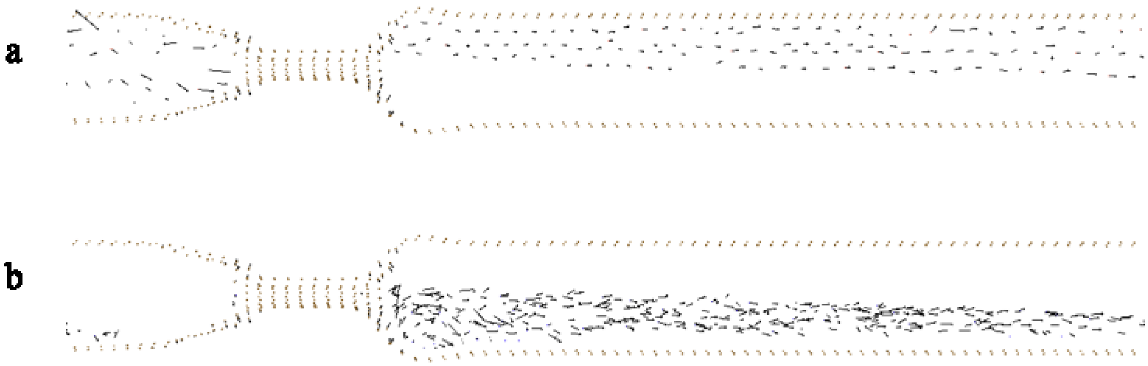

Fig. 9. Vector representation of the (a) gaseous phase and (b) liquid phase in the gas-liquid model, where the length of the vector indicates the velocity.

The liquid phase as shown in Fig. 9 (b) indicates the same flow pattern as in the partially-filled model (Fig. 4) where a vortex is formed in front of the peristaltic wave. With respect to the velocity profile, in our model, the gaseous phase does not influence the liquid flow properties. Also, the mixing profile of the gas-liquid model (Fig. 10), is practically identical to the partially-filled model (Fig. 6 (b)).

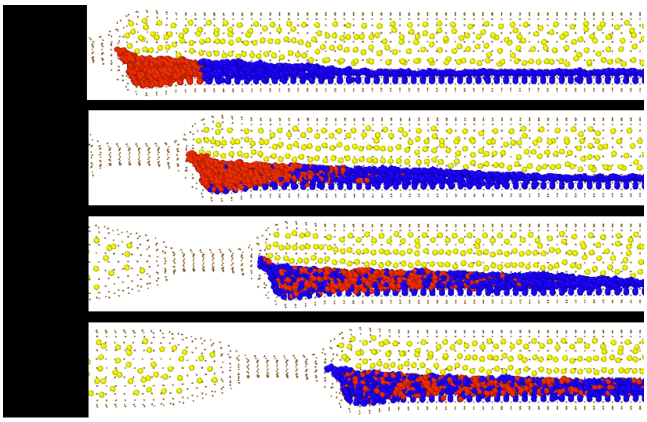

Fig. 10 Mixing profile of gas-liquid model using tracking particles (red coloured) at different time-steps.

3.4. Comparison of the velocity profiles of all three models

The diagrams in Fig. 11 show the axial velocity distribution of the liquid particles along the axial direction at three different time-steps: (a) represents the completely-filled model, (b) the partially-filled model and (c) the gas-liquid model.

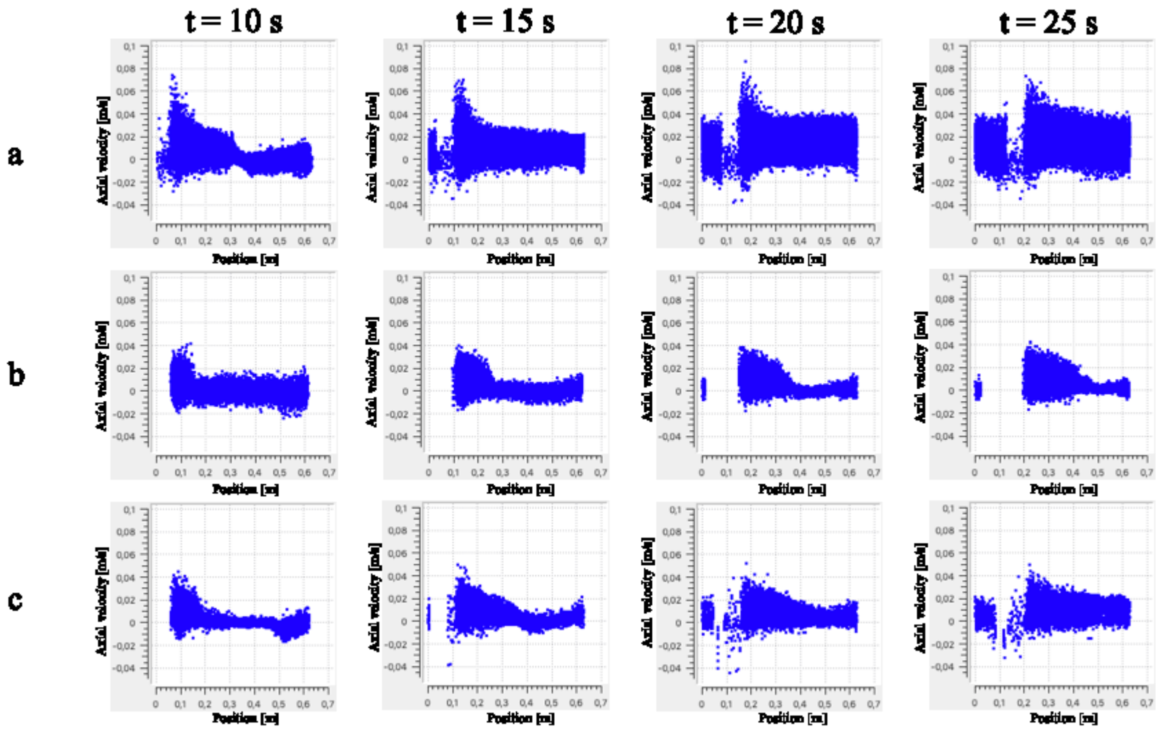

Fig. 11. Graphical representation of the axial velocity along the colon models at different time-steps, where (a) represents the completely-filled model and (b) the partially-filled model and (c) the gas-liquid model.

In all models, the highest velocity magnitude (Fig. 5 and Fig. 8) as well as the highest axial velocities are found in the region right in front of the peristaltic contraction in the DI region. If we compare the three models, we can establish that the maximum axial velocity of the particles representing the liquid is in the completely-filled model, which is approximately twice as high as in the other two models. The axial velocity distribution shows in all models a different pattern, whereas the partially-filled model and the gas-liquid model only show a slight difference.

In the completely-filled model the mean axial velocity distribution increases between 10 and 20 seconds by about 40% and stays constant, whereas the axial velocity distribution in partially-filled model remain almost constant. After 25 seconds the gas-liquid model shows a slight increase in the mean axial velocity.

As the reduction of fluid in the colon model by approximately 60% resulted in a 50% reduced liquid axial velocity. The addition of another fluid – in this case gas particles – suggests that in the gas-liquid model the axial velocity of the liquid is slightly higher than in the partially-filled model without gas.

In terms of dosage forms, the velocities in Fig. 11 explain the result of Fig. 6, Fig. 10 and Fig. 7. The completely-filled model, in fact, shows both higher axial velocities and a larger distribution of axial velocities. This is reflected in a faster propagation of both finely dispersed tracking particles (Fig. 6) and large tablets (Fig. 7), and in the more uniform distribution of particles in Fig. 6.

4. Conclusion

In this study, we develop three different computational models to describe the peristaltic motion in the colon. These models consider different filling levels as well as the presence of the gaseous phase. We also simulated the mixing of fully dispersed tracking particles and the motion of larger tablets.

Our study investigates how the hydrodynamics is influenced by different filling levels and the presence of the gas phase. The filling level in the colon has an influence on the shear stresses, mixing, concentration and the hydrodynamic profiles, which can be highly relevant for medical research as well as pharmaceutical applications. For the disintegration of the dosage form and, thus, the release of drug particles, the existing shear forces and shear rates are one of the critical parameters. Conventional in-vitro dissolution tests for targeted drug delivery predictions are performed under standardised conditions without considering the environmental conditions [30]. Our results show that, when modelling drug dissolution and drug disintegration, environmental conditions play a crucial role. This is true for both the case of solid dosage form (tablet) and fully dispersed form.

The model, therefore, provides a realistic environment for drug dissolution testing compared to the standardised dissolution tests and apparatuses currently in use [30]. In this study, we focus on the two extreme cases of completely dispersed drugs and insoluble tablets, but the model can be further improved by introducing dissolving tables that gradually disintegrate in the luminal content [37]. This also affects the reliability of the prediction of in-vivo performance, which is one of the main focuses in biopharmaceutical research [30]. In fact, computer simulations may in the near future replace the standardised tools that are used.

References

[1] A. Alexiadis (2014) A smoothed particle hydrodynamics and coarse-grained molecular dynamics hybrid technique for modelling elastic particles and breakable capsules under various flow conditions. *International Journal for Numerical Methods in Engineering*, 100, 713-719.

[2] A. Alexiadis (2015) The Discrete Multi-Hybrid System for the Simulation of Solid-Liquid Flows. *PLoS ONE*, 10(5): e0124678.

[3] A. Alexiadis (2015a) A new framework for modelling the dynamics and the breakage of capsules, vesicles and cells in fluid flow. *Procedia IUTAM*, 16, 80-88.

[4] A. Alexiadis, K. Stamatopoulos, W. Wen, H.K. Batchelor, S. Bakalis, M. Barigou, M.J.H. Simmons (2017) Using discrete multi-physics for detailed exploration of hydrodynamics in an in vitro colon system. *Computers in Biology and Medicine,* 81, 188–198.

[5] M. Ariane, A. Alexiadis, M. Barigou, (2016) Smoothed particle hydrodynamic modelling of an aortic valve with flexible leaflets. *ChemEngDay* (Bath United Kingdom).

[6] M. Ariane, M.H. Allouche, M. Bussone, F. Giacosa, F. Bernard, M. Barigou, A. Alexiadis (2017) Discrete multi-physics: A mesh-free model of blood flow in flexible biological valve including solid aggregate formation. *PLoS ONE*, 12(4): e0174795.

[7] M. Ariane, W. Wen, D. Vigolo, A. Brill, F.G.B. Nash, M. Barigou, A. Alexiadis (2017a) Modelling and simulation of flow and agglomeration in deep veins valves using discrete multi physics. *Computers in Biology and Medicine*, 89, 96-103.

[8] M. Ariane, S. Kassinos, S. Velaga, A. Alexiadis (2018) Discrete multi-physics simulations of diffusive and convective mass transfer in boundary layers containing motile cilia in lungs. *Computers in Biology and Medicine*, 95, 34-42.

[9] F. Askevold (1956) Investigation on the influence of diet on the quantity and composition of intestinal gas in humans. *Scandinavian Journal of Clinical & Laboratory Investigation*, 8, 87-94.

[10] P.A. Bampton, P.G Dinning (2013) High Resolution Colonic Manometry – What Have We Learnt? - a Review of the Literature 2012. *Current Gastroenterology Reports*, 15, 328.

[11] G. Bassotti, M. Gaburri (1988) Manometric investigation of high-amplitude propagated contractile activity of the hum an colon. *The American journal of physiology*, 255 (18), G660-G664.

[12] A.E. Bharucha, R.D. Hubmayr, I.J. Ferber, A.R. Zinsmeister (2001) Viscoelastic properties of the human colon. *American Journal of Gastrointestinal and Liver Physiology*, G459-G466.

[13] J. Christensen (1989) Chapter 24 – Handbook of Physiology, The Gastrointestinal System: Colonic Motility. *American Physiological Society*, 939-973.

[14] J. Christensen (1994) Chapter 24 – Physiology of the Gastrointestinal Tract, Third Edition: The motility of the colon. *Raven Press*, 991-1024.

[15] K. Connington, Q. Kang, H. Viswanathan, A. Abdel-Fattah, S. Chen (2009) Peristaltic particle transport using the lattice Boltzmann method. *Physics of Fluids*, 21, 053301.

[16] J.H. Cummings, E.W. Pomare, W.J. Branch, C.P.E. Naylor, G.T. Macfarlane (1987) Short chain fatty acids in human large intestine, portal, hepatic and venous blood. *Gut,* 28, 1221-1227.

[17] J.-H. Chen, Y. Yu, Z. Yang, W.-Z. Yu, W.L. Chen, H. Yu, M.J.-M. Kim, M. Huang, S. Tan, H. Luo, J. Chen, J.D.Z. Chen, J.D. Huizinga (2017) Intraluminal pressure patterns in the human colon assessed by high-resolution manometry. *Scientific Reports,* 7, 41436.

[18] A. Diakidou, M. Vertzoni, K. Goumas, E. Söderlind, B. Abrahamsson, J. Dressman, C. Reppas (2009) Characterization of the Contents of Ascending Colon to Which Drugs are Exposed After Oral Administration to Healthy Adults. *Pharmaceutical Research,* 26(9), 2141-2151.

[19] D.R. Fried (2005) New oral delivery systems for treatment of inflammatory bowel disease. *Advanced Drug Delivery Reviews,* 57, 247-265.

[20] G.C. Ganzenmüller, M.O. Steinhauser, P. Van Liedekerke, K.U. Leuven (2011) The Implementation of Smoothed Particle Hydrodynamics in LAMMPS. *Retrieved from (lammps.sandia.gov/doc/PDF/SPH_LAMMPS_userguide.pdf),* (last accessed 17.10.2019).

[21] R. Goffredo, A. Pecora, L. Maiolo, A. Ferrone, E. Guglielmelli, D. Accoto (2016) A Swallowable Smart Pill for Local Drug Delivery. *Journal of Microelectromechanical Systems*, 25 (2), 362-370.

[22] M. Kot, H. Nagahashi, P. Szymczak (2015) Elastic moduli of simple mass spring models. *The Visual Computer*, 31 (10), 1339-1350.

[23] S. Paradeep Kumar, D. Prathibha, R. Parthibarajan, C. Rubina Reichal (2012) Novel Colon Specific Drug Delivery System: A Review. *International Journal of Pharmacy and Pharmaceutical Siences,* 4 (1), 22-29.

[24] S. Kurbel, B. Kurbel, A. Včev (2006) Intestinal gases and flatulence: Possible causes of occurrence. *Medical Hypotheses,* 67, 235-239.

[25] A. Lamprecht, N. Ubrich, H. Yamamoto, U. Schäfer, H. Takeuchi, P. Maincent, Y. Kawashima, C.-M. Lehr (2001) Biodegradable Nanoparticles for Treated Drug Delivery in Treatment of Inflammatory Bowel Disease. *Journal of Pharmacology and Experimental Therapeutics,* 299 (2), 755-781.

[26] J. Lee (2003) Drug Nano- and Microparticles Processed into Solid Dosage Forms: Physical Properties. *Journal of Pharmaceutical Sciences,* 92 (10), 2057-2068.

[27] O. Liem, R.E. Burgers, F.L. Connor, M.A. Benninga, S.N. Reddy, H.M. Mousa, C. Di Lorenzo (2012) Solid-state vs water-perfused catheters to measure colonic high-amplitude propagating contractions. *Neurogastroenterology and Motility,* 24, 345-e167.

[28] G.R. Liu, M.B. Liu (2003) Smoothed Particle Hydrodynamics: a Meshfree Particle Method. *World Scientific Publishing, Singapore.*

[29] B.A. Lloyd, G. Székely, M. Harders (2007) Identification of Spring Parameters for Deformable Object Simulation. *IEEE Transactions on Visualization and Computer Graphics,* 13 (5), 1081-1094.

[30] M. Long, Y. Chen (2009) Chapter 14 – Developing Solid Oral Dosage Forms, Dissolution Testing of Solid Products. *Academic Press.*

[31] notstarman (2007) Lower GI Movies – Peristalsis. *[online video] Available at: <https://www.youtube.com/watch?v=Ctp2BHimmLk>,* [Accessed 12/03/2018].

[32] notstarman (2007) Lower GI Movies – segmentation in jejunum. *[online video] Available at: <https://www.youtube.com/watch?v=GdNtRom-Pvs>,* [Accessed 12/03/2018].

[33] A. Pazdniakou, P.M. Adler (2012) Lattice Spring Models. *Transport Porous Media*, 93, 243-262.

[34] A.B. Pithadia, S. Jain (2011) Treatment of inflammatory bowel disease (IBD). *Pharmacological Reports*, 63, 629-642.

[35] S. Plimpton (1995) Fast parallel algorithms for short-range molecular dynamics. *Journal of Computational Physics,* 117, 1-19.

[36] V.V. Prasanth, R. Jayaprakash, S.T. Mathew (2012) Colon Specific Drug Delivery Systems: A Review on Various Pharmaceutical Approaches. *Journal of Applied Pharmaceutical Science,* 2, 163-169.

[37] A. Rahmat, M. Barigou, A. Alexiadis (2019) Numerical simulation of dissolution of solid particles in fluid flow using the SPH method. *International Journal of Numerical Methods for Heat & Fluid Flow*, 30(1), 290-307.

[38] S.K. Sarna (2010) Colonic Motility: From Bench Side to Bedside. *San Rafael (CA): Morgan & Claypool Life Sciences*.

[39] C. Schiller, C.-P. Fröhlich, T. Giessmann, W. Siegmund, H. Mönnikes, N. Hosten, W. Weitschies (2005) Intestinal fluid volumes and transit of dosage forms as assessed by magnetic resonance imaging. *Alimentary Pharmacology & Therapeutics*, 22, 971-979.

[40] M.D. Sinnot, P.W. Cleary, J.W. Arkwright, P.G. Dinning (2012) Investigating the relationships between peristaltic contraction and fluid transport in the human colon using Smoothed Particle Hydrodynamics. *Computers in Biology and Medicine*, 42, 492-503.

[41] M.D. Sinnot, P.W. Cleary, P.G. Dinning, J.W. Arkwright, M. Costa (2015) Interpreting manometric signals for propulsion in the gut. *Computational Particle Mechanics*, 2, 273-282.

[42] K. Stamatopoulos, H. Batchelor, M.J.H. Simmons (2016) Dissolution profile of theophylline modified release tablets, using a biorelevant Dynamic Colon Model (DCM). *European Journal of Pharmaceutics and Biopharmaceutics*, 108, 9-17.

[43] A. Stukowski (2010) Visualization and analysis of atomistic simulation data with OVITO – the Open Visualization Tool, *Modelling Simulation Materials Science and Engineering*, 18, 015012

[44] P.J. Watts, L. Illum (1997) Colonic Drug Delivery. *Drug Development and Industrial Pharmacy*, 23(9), 893-913.